State-selective predissociation dynamics of methylamines: The vibronic and H/D effects on the conical intersection dynamics

Doo-Sik Ahn,[1] Jeongmook Lee,[1] Jeong-Mo Choi,[1] Kyoung-Seok Lee,[1,a)] Sun Jong Baek,[1] Kunhye Lee,[2] Kyoung-Koo Baeck,[2] and Sang Kyu Kim[1,b)]
[1]*Department of Chemistry and School of Molecular Science (BK21), KAIST, Daejeon 305-701, Republic of Korea*
[2]*Department of Chemistry, Kangnung University, Gangwon Do 210-702, Republic of Korea*

(Received 26 February 2008; accepted 6 May 2008; published online 11 June 2008)

The photodissociation dynamics of methylamines (CH_3NH_2 and CD_3ND_2) on the first electronically excited state has been investigated using the velocity map ion imaging technique probing the H or D fragment. Two distinct velocity components are found in the H(D) translational energy distribution, implying the existence of two different reaction pathways for the bond dissociation. The high H(D) velocity component with the small internal energy of the radical fragment is ascribed to the N–H(D) fragmentation via the coupling of S_1 to the upper-lying S_2 repulsive potential energy surface along the N–H(D) bond elongation axis. Dissociation on the ground S_0 state prepared via the nonadiabatic dynamics at the conical intersection should be responsible for the slow H(D) fragment. Several S_1 vibronic states of methylamines including the zero-point level and $n\nu_9$ states ($n=1$, 2, or 3) are exclusively chosen in order to explore the effect of the initial quantum content on the chemical reaction dynamics. The branching ratio of the fast and slow components is found to be sensitive to the initial vibronic state for the N–H bond dissociation of CH_3NH_2, whereas it is little affected in the N–D dissociation event of CD_3ND_2. The fast component is found to be more dominant in the translational distribution of D from CD_3ND_2 than it is in that of H from CH_3NH_2. The experimental result is discussed with a plausible mechanism of the conical intersection dynamics. © *2008 American Institute of Physics*. [DOI: 10.1063/1.2937451]

I. INTRODUCTION

The spectroscopic and dynamic studies of small molecular systems offer the great opportunity to interrogate the state-selective chemistry where the specific quantum mechanical state may play a unique role in chemical reaction dynamics. State-to-state reaction dynamics of small molecules, therefore, have been both intensively and extensively studied for decades.[1–9] In the half-collision experiment, for instance, the specific quantum state of the reactant is prepared via the one-photon or double-resonance excitation using the properly tuned laser pulses, and it is followed by the probing of the specific quantum mechanical state of the product. The product state distribution reflects the dynamics taking place between reactants and products, and the information about the detailed potential energy surfaces can be inferred from the experimental results. These studies include those both in the frequency and time domains. Through the integrated researches using a variety of experimental tools, many interesting and important aspects of chemical dynamics have been revealed for a number of small molecular systems in the recent decades.[9–12] And yet, since the potential energy surface is multidimensional and it becomes more complex as the number of atoms increases, the dynamics of not-so-small but not-that-large chemical systems are still quite poorly understood in terms of the state selectivity in many chemical reactions.[13–16] In order to understand the detailed dynamics of such complex polyatomic systems, one needs to archive the knowledge of many facets of the multidimensional dynamical phenomena. In this aspect, the study of methylamines, which is a seven-atomic molecular system, seems to be quite appropriate for the endeavor along this direction. Moreover, methylamines are obviously quite common in organic and biological building blocks and play the essential role as a Lewis base or hydrogen-bonding donor. Dynamic study of methylamine will be thus quite useful in better understanding of photochemistry and photobiology especially occurring at UV wavelengths where the amino moiety may act as a photon catcher.

In this work, we explore the state-selective predissociation dynamics of methylamines.[17–21] There had long been many studies on the bond dissociation dynamics of methylamines. These include the mass-selected translational energy measurements of all fragments at 222 nm by Waschewsky *et al.*,[17] the Rydberg-tagged hydrogen translational energy measurement by Ashfold and co-workers,[18,19] the theoretical calculation of the excited potential energy surfaces by Dunn and Morokuma,[20] and the more recent stimulated Raman excitation study by Golan *et al.*,[21] Most of the previous studies except the latest one, however, had been done without the proper characterization of the initial quantum state of methylamines on the S_1 state. The S_1 state spectroscopy has recently been thoroughly investigated by our group and the

a)Permanent address: Korea Research Institute of Standards and Science, Daejeon 305-340, Republic of Korea.
b)Author to whom correspondence should be addressed. Electronic mail: sangkyukim@kaist.ac.kr.

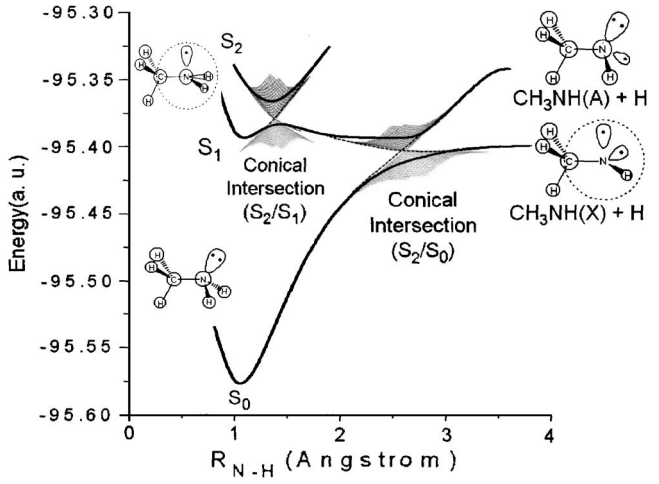

FIG. 1. Potential energy curves showing two conical intersections along the N–H bond dissociation coordinate. The crossing occurs at the planar geometry, where the NH_2 plane is along the C–N axis.

complicated band contours associated with the S_1-S_0 transition have been unambiguously assigned using the internal/overall rotational Hamiltonian matrix.[22–24]

The S_1-S_0 optical transition belongs to the n-3s Rydberg type though the optically prepared state is immediately coupled to nearby valence excited states. Namely, even at the zero-point energy level of the S_1 state, the ultrafast N–H bond rupture takes place giving the S_1 state lifetime less than a few hundred femtoseconds, resulting in the very broad band in the resonantly enhanced multiphoton-ionization (REMPI) spectrum. The mode dependence on the photoionization efficiency of CH_3NH_2 observed by Golan *et al.*[21] is consistent with the fact that the N–H dissociation is fast enough so that the memory of the particular mode attained via the Franck–Condon transition may persist during the dephasing process. The N–H bond dissociation takes place via tunneling at the S_1 zero-point state as clearly manifested by the huge NH/ND isotope substitution effect on the predissociaton lifetime. The H/D isotope substitution on the methyl moiety show little effect on the excited state lifetime, indicating that the main dephasing channel should be the N–H(D) dissociation. Based on the spectroscopic characterization of all H/D isotope analogs of methylamine, the N–H(D) bond dissociation dynamics starting from various S_1 quantum states are explored here for CH_3NH_2 and CD_3ND_2. Using the velocity map ion imaging technique, we have determined the translation energy distribution of the H(D) fragment in the three-dimensional space. The dissociation dynamics especially at the conical intersection where the bifurcation of the wavepacket occurs is discussed. High level *ab initio* calculations are also carried out for the construction of the adiabatic potential energy surface along the dissociating coordinate.

II. EXPERIMENT

Methylamine (Aldrich) was mixed with a Ne carrier gas with a seeding percentage of 7%. The gas mixture was then expanded into vacuum through a 0.3 mm diameter nozzle orifice (General Valve series 9). The vacuum chamber was

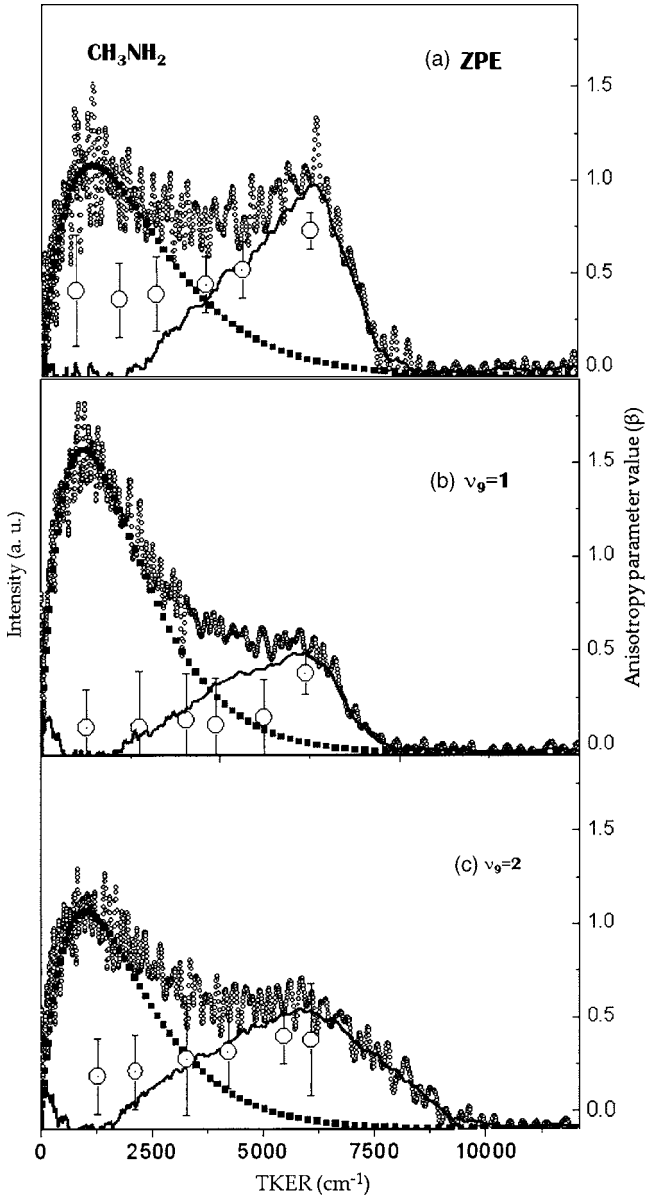

FIG. 2. Total translational energy distribution and anisotropy parameter values from the CH_3NH_2 dissociation excited at the (a) ZPE, (b) $\nu_9=1$, and (c) $\nu_9=2$ levels of the S_1 state.

equipped with two turbopumps, and the background pressure was maintained at mid-10^{-8} Torr when the nozzle was operated at 10 Hz. The molecular beam was skimmed though a 1 mm diameter skimmer (Precision Instrument) prior to being overlapped with the exciting laser pulses. The third harmonic output of the neodynium doped yttrium aluminum garnet (Spectra-Physics, GR150) was used to pump two independent dye lasers in order to generate the pump laser pulse in the 232–240 nm range and the probe laser around 243.1 nm for the (2+1) ionization of the H(D) fragment. The H(D) fragment ion was repelled, accelerated, drifted along the time-of-flight axis and detected via the microchannel plate equipped position-sensitive detector (Burl, 40 mm diameter, P20 phosphor screen). Electric fields applied to the nongrid ion optics were carefully adjusted for the appropriate velocity-mapping condition.[25,26] The pump laser polarization was perpendicular to the time-of-flight axis and parallel to

TABLE I. Relative yields of the slow and fast components, maximum energies in the translational energy distribution, translational temperatures, and average kinetic energies measured at the S_1 zero-point state and $n\nu_9$ states of CH_3ND_2 and CD_3ND_2.

n	Pump energy (cm^{-1})	Yields A_{slow}/A_{fast}	Maximum total kinetic energy (cm^{-1})	Translational temperature[a] (K)	Average kinetic energy[b] (cm^{-1})
			CH_3NH_2		
0	41 676	0.54/0.46	7500 ± 400	2250 ± 200	4860
1	42 314	0.78/0.22	8000 ± 400	2300 ± 220	5090
2	42 959	0.48/0.52	8750 ± 400	2300 ± 230	5560
			CD_3ND_2		
0	42 139	0.30/0.70	6750 ± 400	1600 ± 200	5070
1	42 595	0.36/0.64	7100 ± 400	1500 ± 180	5100
2	43 081	0.34/0.66	7750 ± 400	1600 ± 180	5380
3	43 541	0.38/0.62	8250 ± 400	1800 ± 180	5420

[a]The slow component of the total translational energy distribution has been reproduced with the following Maxwell–Boltzmann distribution: $f(E)dE=2(E/\pi(kT)^3)^{1/2}\exp(-E/KT)dE$.
[b]For the fast component only.

the position-sensitive detector to ensure the cylindrical symmetry of the fragmentation with respect to the ion detection. The image was taken by a charge coupled device camera (Hamamatsu) with the event-counting method. In order to cover the entire Doppler width of the H(D) fragment transition, the probe laser was continuously scanned while the ion image was averaged over 36 000 laser shots. Raw images were reconstructed through the basis set expansion algorithm.[27] The translational energy scale in the image was calibrated using the O_2 photodissociation. Computationally, the one-dimensional potential energy curves involved in the S_1 predissociation dynamics are calculated at the coupled cluster singles and doubles (CCSD) level [6-311++G(d,p)] for the ground state and at the equation-of-motion (EOM) CCSD for the excited state. The ACESII quantum mechanical calculation program was used.[28] The molecular structure at the conical intersection was predicted with a multireferenced wavefunction [complete active space self-consistent field (CASSCF)]. This calculation was performed with the GAUSSIAN03 set of programs.[29]

III. RESULTS AND DISCUSSION

It is well accepted now that methylamines on the S_1 state predissociate via the vibronic coupling to the $n\sigma^*$(N–H) S_2 state, which is repulsive in nature along the N–H elongation axis. At the zero-point level of the S_1 state, such a fast coupling occurs via tunneling through a reaction barrier which is generated by the avoided crossing of two diabatic surfaces. As the reaction proceeds on the repulsive potential curve, another conical intersection is encountered since the repulsive S_2 state correlates to the ground state of the CH_3NH fragment, whereas the ground electronic state diabatically correlates to the excited CH_3NH at the asymptotic limit (Fig. 1). This S_2/S_0 conical intersection then plays an essential role in the bifurcation dynamics of the wavepacket sliding on the potential energy curve along the N–H coordinate.

In Fig. 2(a), the total translational energy distribution, deduced from the H fragment kinetic energy distribution using the simple kinematics, for the dissociation at the S_1 zero-point level is shown. The maximum energy of the distribution provides the upper limit of the N–H bond dissociation energy of 34 250 ± 400 cm^{-1}, which is consistent with the earlier reported value of 34 550 ± 200 cm^{-1}.[18] Two distinct bimodal distributions are observed, which had also been observed in previous other studies. Since it has been proven, through many spectroscopic and dynamics studies, that the source of the H fragment is only the N–H dissociation at UV excitation wavelengths near the S_1 zero-point level, the bimodal translational distribution indicates that there are two distinct reaction pathways for the N–H bond dissociation. At the low energy region, the distribution has the Boltzmann-like shape suggesting that the internal energy of the CH_3NH fragment is quite randomized. Meanwhile, the distribution found at the higher energy region shows the sharply rising edge at the high kinetic energy, indicating that the N–H bond rupture is very fast, leaving only the small energy to the internal degrees of freedom of CH_3NH. The Maxwell–Boltzmann distribution function with an adjustable parameter of the translational temperature is used for reproducing the slow component, whereas the fast component is represented by a curve connecting averaged values of the distribution which is obtained by subtraction of the corresponding Maxwell–Boltzmann distribution function from the total experimental distribution, giving the translational temperature of 2250 ± 200 K and average translational energy of 4860 cm^{-1} for the slow and fast components, respectively. The translational temperatures for the slow components and average kinetic energies for the fast components of all the distributions measured in this work are listed in Table I. Both the translational temperature and average kinetic energy of the respective slow and fast components show the increase as the available energy increases, as expected.

Considering the small vibrational excitation of the CH_3NH fragment, the fast H component should come from the ultrafast bond dissociation on the repulsive S_2 state. Following the S_1-S_2 tunneling process, the reaction occurs on the diabatic potential energy surface. Therefore, there is not enough time for the energy to be randomized among the

TABLE II. Calculated energetics of methylamines and methylamino radicals using the CCSD method [6-31++G(d,p)] for the ground state and the EOM-CCSD for the excited state.

Methylamines	CH_3NH_2	CD_3ND_2
Energy(S_0)+ZPE (hartree)	−95.521 656	−95.538 385
Energy(S_1)+ZPE (hartree)	−95.339 568	−95.354 887
Adiabatic transition energy (cm^{-1})	39 967	41 079
D_0 (cm^{-1})	32 242	34 280
Experimental D_0 (cm^{-1})[a]	34 250 ± 400	35 350 ± 400
N–H(D) predissociation barrier (cm^{-1})	2 568	4 053
Methylamino radical	CH_3NH	CD_3ND
Energy(X)+ZPE (hartree)	−95.374 749	−95.381 703
Vertical A-X excitation energy (cm^{-1})[b]	12 664	12 664

[a]This work.
[b]ZPE is not included.

internal degrees of freedom of the reactant. Meanwhile, there are two possible mechanisms for the slow H component of the translational energy distribution. One is the internal conversion from S_1 to vibrationally hot S_0 state, which is followed by the unimolecular dissociation giving rise to the products of which the energy is statistically distributed. The other mechanism would be the internal conversion taking place at the S_2/S_0 conical intersection.[18] Since the $\tilde{A}$ state of the CH_3NH radical, the adiabatically correlated product from S_2, is not energetically accessible at the S_1 zero-point level excitation,[20] the wavepacket trapped in the upper cone of the conical intersection may undergo the nonadiabatic transition to the vibrationally hot S_0 state. Our CCSD calculation shows that the vertical $\tilde{A}$-$\tilde{X}$ excitation energy of the CH_3NH radical is 12 664 cm^{-1} (Table II). The S_0-S_1 direct mechanism requires the very fast internal conversion rate which should be comparable to the rate of tunneling. The lifetime of the S_1 zero-point level had been estimated to be less than 300 fs from its spectral width in the REMPI spectrum.[22] The almost equal ratio of the slow and fast components in the distribution in Fig. 2(a) implies then that the S_0-S_1 internal conversion rate has to be $\sim 10^{12}$ S^{-1}, which is unusually high for the rate of the nonradiative process.

In the case of CD_3ND_2, the D fragment shows the translational energy distribution similar to that of H from CH_3NH_2 at its S_1 zero-point level [Fig. 3(a)]. In the photodissociation of CD_3ND_2, the fast velocity component is found to be more dominant than the slow component. The edge at the maximum kinetic energy shows a sharp rise, indicating that the prompt N–D dissociation carries the most of available energy into the translational energy of fragments. The estimated N–D dissociation energy is 35 350 ± 400 cm^{-1}, which is quite reasonable considering the zero-point energy difference of CD_3ND_2 and CH_3NH_2 (Table I). The lifetime of the S_1 zero-point state of CD_3ND_2 had been estimated to be around ~8 ps,[30] which is about 20 times longer than that of CH_3NH_2. This fact indicates, if the S_0-S_1 direct mechanism is mainly responsible for the slow D, that the S_1-S_0 internal conversion rate of CD_3ND_2 should be comparable to or slightly slower than the S_1-S_2 tunneling rate and therefore that it should be 20 times slower than the internal conversion rate of CH_3NH_2. However, the much higher density of states of CD_3ND_2 in the ground state compared to that of CH_3NH_2 predicts the opposite case. The H/D substitution effect on the tunneling is expected to be huge, as clearly shown for predissociation lifetimes of CH_3NH_2 and CD_3ND_2. On the other hand, the H/D effect on the internal conversion rate is expected to be less dramatic, and moreover the trends of two processes are often opposite each other. These experimental observations make us exclude the possibility of the major role of S_0-S_1 internal conversion process in the first electronically excited state of methylamines.

The other plausible source for the slow H(D) fragment is then the vibrationally hot ground state molecules generated

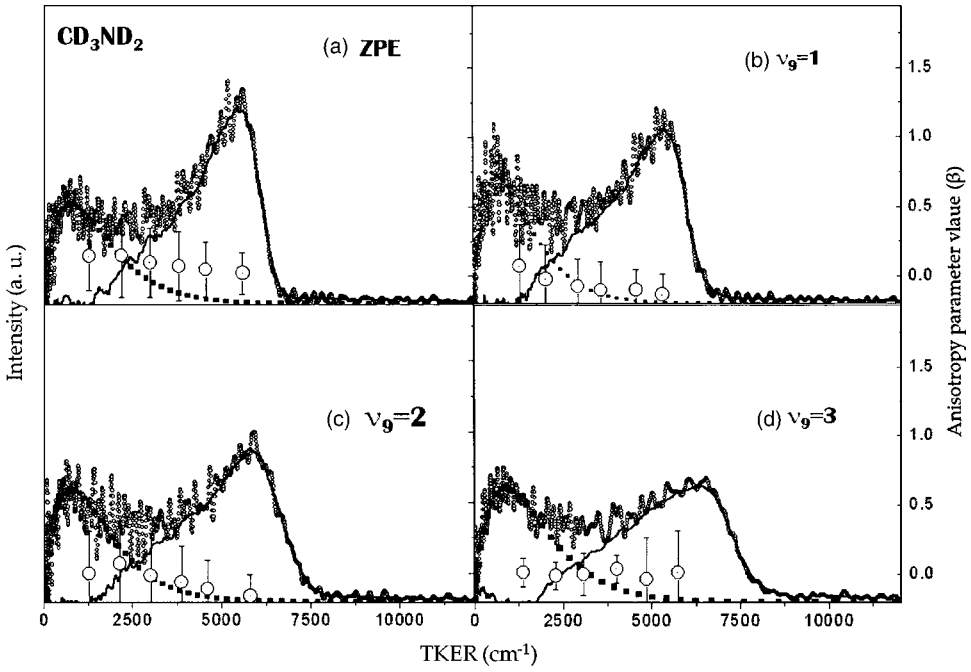

FIG. 3. Total translational energy distributions and anisotropy parameter values from the CD_3ND_2 dissociation excited at the (a) ZPE, (b) $\nu_9=1$, (c) $\nu_9=2$, and (d) $\nu_9=3$ levels of the S_1 state.

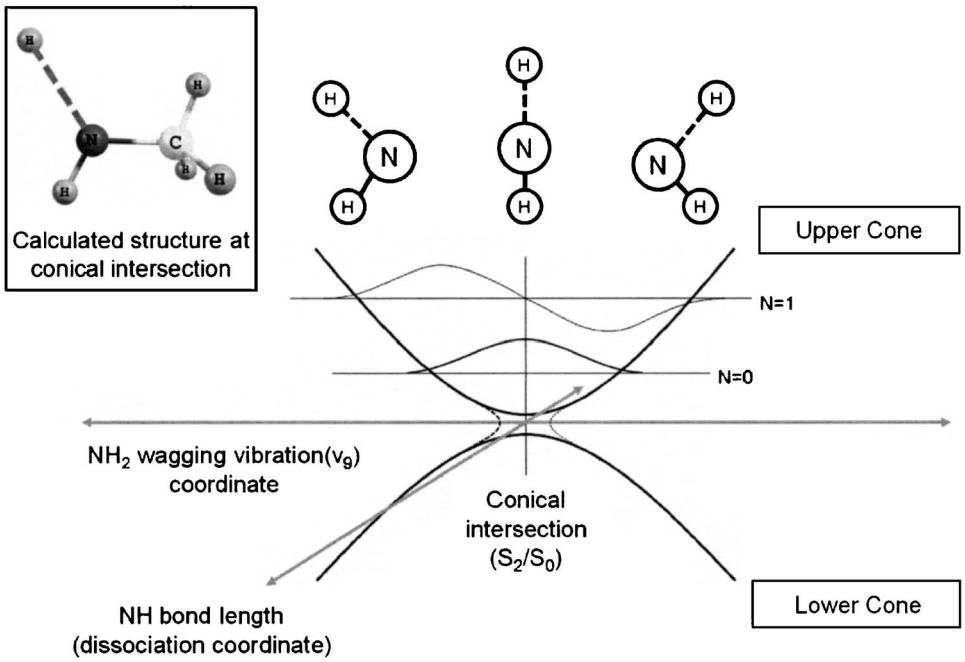

FIG. 4. Schematic diagram of the one-dimensional cut of the two-dimensional potential energy surface showing the CASSCF calculated geometry at the conical intersection. The N–H bond elongation axis is perpendicular to the paper.

by the dynamics at the S_2/S_0 conical intersection as noted earlier and also been proposed by Ashfold and co-workers in their NH_3 photodissociation studies.[31,32] Since the first electronically excited CH_3NH is not energetically accessible at excitation energies employed in this work (Table II), the wavepacket following the adiabatic potential curve will be bounced off the potential wall on the product side, leaking into the vibrationally hot ground state, and finally leading to the products of which the energy is statistically distributed among all degrees of freedom. In this case, the slow and fast H(D) components in the translational energy distribution reflect the bifurcation dynamics occurring at the S_2/S_0 conical intersection. Very similarly to the case of ammonia of which the dynamics have recently been thoroughly studied by Ashfold and co-workers[31,32] and Crim and co-workers,[33–36] the conical intersection along the N–H bond elongation axis is formed when the NH_2 plane is oriented along the C–N axis. The barrier for the torsional motion about the C–N bond had been determined to be very small to give 5 cm^{-1} at the S_1 zero-point state,[22] and it seems to be quite reasonable to treat the torsional mode about C–N in the excited state as one corresponding to the internal free rotation. Accordingly, the internal rotation about the C–N bond does not affect the dynamics at the conical intersection since there would be no torque exerted along the torsional coordinate during the dissociation process. Though chemical reactions of polyatomic molecules such as methylamines need the multidimensional potential energy surface for the understanding of dynamics, it is very useful to consider the potential energy surface in the reduced dimensionality. Accordingly, in the two-dimensional potential energy surfaces, the N–H bond axis is one of the coordinates along which the reaction proceeds, whereas the wagging angle of the NH_2 plane with respect to the C–N axis would be another coordinate which does affect the conical intersection dynamics (Fig. 4).

In the ground state of methylamines, the NH_2 moiety is bent with respect to the C–N axis, whereas it becomes planar on the S_1 state. Because of this structural change upon the S_1-S_0 optical transition, the NH_2 wagging mode (ν_9) is much activated in the S_1 state. The translational energy distribution of H from the $1\nu_9$ state of S_1 is shown in Fig. 2(b). The most dramatic change from the distribution in Fig. 2(a) is that the fast velocity component has been much decreased whereas the slow component becomes dominant. This suggests that the vibrational excitation of the NH_2 wagging mode in the S_1 state is highly influential on the bifurcation dynamics at the conical intersection. Even though the NH_2 wagging mode is the disappearing mode eventually at the asymptotic limit, it seems to be sustained at the conical intersection. The planarity of the NH_2 moiety at the conical intersection had been theoretically predicted by Dunn and Morokuma,[20] which is also confirmed here at the CASSCF(6,6)/6-31+G(d) level of theory. From the qualitative picture of the simple wavepacket propagation model, the wavepacket containing one quantum of NH_2 wag will have a node at the point of conical intersection along the angle of the NH_2 plane with respect to the C–N axis. Thus the probability of the diabatic passage through the conical intersection to the products is expected to be diminished at the $\nu_9=1$ state compared to that at the zero-point state. Meanwhile, the portion of the wavepacket trapped in the upper cone will dephase and leak to the S_0 ground state where the vibrationall hot molecules dissociate in a statistical way. This conical intersection mechanism explains the experimental result quite well at least qualitatively. When the $\nu_9=2$ state of S_1 is excited, it has been found that the relative portion of the fast component is slightly larger than that from the $\nu_9=1$ state, whereas it is still smaller than that from the zero-point state, Fig. 2(c). This experimental fact also supports the above mechanism. Namely, as two nodes of the $\nu_9=2$ wavepacket do not coincide with the conical intersection, the diabatic passage at the conical intersection into products is more probable compared to that at the $\nu_9=1$ state, while it is less probable than it is for the zero-point state where the wavepacket is localized at the conical

intersection. Assuming that the slow channel follows the Boltzmann statistics, all the translational distributions are deconvoluted to give the relative yields of the slow and fast components at each excitation wavelength (Table I). Even though these estimated values have large uncertainties, the dynamic trend is consistent with the above mechanism. This is also in accord with the recent theoretical study for the O–H bond dissociation of phenol by Lan *et al.*[37] in terms of the even/odd mode effect on the conical intersection dynamics. The anisotropy parameters are found to vary from 0.2 to 1.0 as a function of the translational energy, indicating that the N–H bond rupture is fast enough that the angular anisotropy of fragments is not washed out due to the overall rotation of the reactant at least for the fast component (Fig. 2). The quantitative analysis of the anisotropy parameter has not been tried here since so many unknown dynamical parameters are involved in the experimental values.

Interestingly, the translational energy distribution of the CD_3ND_2 dissociation does not show the mode dependence (Fig. 3). The branching ratios of the slow and fast components of the distributions are more or less the same for all excitation states of $n\nu_9$ $(n=0,1,2,3)$ employed here besides the increase in the maximum translation energy as the excitation energy increases. The much slower N–D dissociation of CD_3ND_2 ($\tau \sim 2-10$ ps) compared to the N–H dissociation of CH_3NH_2 ($\tau \sim 0.2-0.3$ ps) should be responsible for such a mode independent behavior. It also appears in the anisotropy parameter, which is found to be nearly zero in the entire energy region (Fig. 3). Namely, as the reaction goes slowly, the memory of the initial S_1 quantum state is lost because of the fast dephasing processes. The faster intramolecular vibrational redistribution due to the higher density of S_1 states of CD_3ND_2 compared to CH_3NH_2 may also contribute to the early washout of the initial quantum state memory. The gradual increase in the slow component with increasing the total energy (Fig. 3) could be ascribed to the increase in the momentum of the wavepacket bouncing off the potential wall of the upper cone which eventually goes back to the S_0 reactant states.

It should also be noted that the fast component is larger than the slow component in the translational energy distributions from CD_3ND_2 at all excitation energies in this work (Fig. 3 and Table I). For instance, at the S_1 zero-point state, the relative yield of the fast component is estimated to be 0.70 for CD_3ND_2, whereas it is 0.46 for CH_3NH_2. According to the mechanism based on the conical intersection dynamics, this means that the diabatic passage of the wavepacket directly into products is more favored for the dissociation of CD_3ND_2 compared to that of CH_3NH_2. This experimental fact is quite interesting since it may give another clue for understanding the nature of the conical intersection in terms of the density of states, H/D tunneling effect, or zero-point energy difference. For the density of states or H/D tunneling effect, even though the number of ways for the molecule to pass through the conical intersection may vary as the density of states or tunneling rate changes by the H/D substitution, one cannot rationalize the preference of one direction over the other direction along the reaction coordinate. For the zero-point energy, however, the H/D substitution may give the substantial difference in the energy gap of two adiabatic potential energy curves at the conical intersection geometry. In the adiabatic picture, the zero-point energy in the potential energy surfaces of the upper cone is much smaller for CD_3ND_2 compared to that for CH_3NH_2. Since the H/D substitution effect on the zero-point energy also applies to the lower cone at the same three-dimensional geometry, one expects little difference in the zero-point energy gaps of the upper and lower cones for CD_3ND_2 and CH_3NH_2. However, it should be noted that in the lower cone, vibrational frequencies along the dissociating N–H(D) as well as $NH_2(ND_2)$ wagging coordinates are imaginary, meaning that one of the N–H(D) stretching modes and $NH_2(ND_2)$ wagging mode should be dropped in the calculation of the zero-point energy. The decrease in the energy gap between the upper and lower cones by removing these imaginary frequencies of the lower cone is relatively larger for CH_3NH_2 compared to that for CD_3ND_2, resulting in the smaller energy gap for CD_3ND_2. Therefore, in the adiabatic picture, the effective energy gap breaking the Born–Oppenheimer approximation at the geometry of the conical intersection is smaller for CD_3ND_2 compared to that for CH_3NH_2. The smaller energy gap provides the stronger vibronic coupling of the upper and lower states, and it may contribute to facilitate the nonadiabatic passage on the actual conical intersection. Even though this explanation for the experiment is only qualitative and quite simplified, it still motivates the more thorough investigation of the zero-point energy effect on the conical intersection dynamics both experimentally and theoretically.

IV. CONCLUSION

It has been found that the S_2/S_0 conical intersection plays a major role in the N–H(D) bond dissociation dynamics of CH_3NH_2 and CD_3ND_2. The fast and slow fragments found in the translational energy distributions originate from different reaction pathways to each other. The fast fragment is the consequence of the diabatic passage of the sliding wavepacket on the repulsive surface at the conical intersection along the N–H(D) reaction coordinate. The slow component is ascribed to the dissociation in the vibrationally hot S_0 state which is populated via the nonadiabatic conversion of the trapped wavepacket in the upper cone at the S_2/S_0 conical intersection. Initial S_1 vibronic excitation of the NH_2 (or ND_2) wagging mode is found to be quite influential on the conical intersection dynamics for CH_3NH_2, while it affects little in the dissociation of CD_3ND_2. The much slower tunneling rate in the N–D dissociation compared to that of N–H should be responsible for the washout of the initial quantum memory in the CD_3ND_2 photodissociation dynamics. The conceptual approach based on a simple wavepacket propagation model in the two-dimensional potential energy surfaces explains the experimental result well qualitatively. The zero-point energy consideration at the conical intersection turns out to be quite helpful in understanding the H/D isotope substitution effect on the conical intersection dynamics. The construction of the detailed potential energy surfaces

in the vicinity of the conical intersection would be desirable for the better understanding of the zero-point energy effect on the conical intersection dynamics.

ACKNOWLEDGMENTS

This work was supported by KOSEF (M10703000936-07M0300-93610 and R01-2007-000-10766-0), SRC/ERC (R11-2007-012-01002-0), Echo technopia 21 project of KI-EST (102-071-606), and KISTI supercomputing center (KSC-2007-S00-2010).

[1] R. Schinke, Photodissociation Dynamics (Cambridge University Press, New York, 1993).
[2] Y.-P. Lee, Annu. Rev. Phys. Chem. **54**, 215 (2003).
[3] H. Sato, Chem. Rev. (Washington, D.C.) **101**, 2687 (2001).
[4] M. Silva, R. Jongma, R. W. Field, and A. M. Wodtke, Annu. Rev. Phys. Chem. **52**, 811 (2001).
[5] R. N. Zare, Science **279**, 1875 (1998).
[6] I. Bar and S. Rosenwaks, Int. Rev. Phys. Chem. **20**, 711 (2001).
[7] F. F. Crim, J. Phys. Chem. **100**, 12725 (1996).
[8] F. F. Crim, Acc. Chem. Res. **32**, 877 (1999).
[9] M. N. R. Ashfold, N. H. Nahler, A. J. Orr-Ewing, O. P. J. Vieuxmaire, R. L. Toomes, T. N. Kitsopoulos, I. A. Garcia, D. A. Chestakov, S. M. Wu, and D. H. Parker, Phys. Chem. Chem. Phys. **8**, 26 (2006).
[10] A. G. Suits, S. D. Chambreau, and S. A. Lahankar, Int. Rev. Phys. Chem. **26**, 585 (2007).
[11] L. J. Butler and D. M. Neumark, J. Phys. Chem. **100**, 12801 (1996).
[12] X. Yang, Int. Rev. Phys. Chem. **24**, 37 (2005).
[13] J. Wei, J. Riedel, A. Kuczmann, F. Renth, and F. Temps, Faraday Discuss. **127**, 267 (2004).
[14] J. S. Lim, Y. S. Lee, and S. K. Kim, Angew. Chem., Int. Ed. **47**, 1853 (2008).
[15] J. S. Lim, I. S. Lim, K. S. Lee, D. S. Ahn, Y. S. Lee, and S. K. Kim, Angew. Chem., Int. Ed. **45**, 6290 (2006).
[16] I. S. Lim, J. S. Lim, Y. S. Lee, and S. K. Kim, J. Chem. Phys. **126**, 034306 (2007).
[17] G. C. G. Waschewsky, D. C. Kitchen, P. W. Browning, and L. J. Butler, J. Phys. Chem. **99**, 2635 (1995).
[18] C. L. Reed, M. Kono, and M. N. R. Ashfold, J. Chem. Soc., Faraday Trans. **92**, 4897 (1996).
[19] M. N. R. Ashfold, R. N. Dixon, M. Kono, D. H. Mordaunt, and C. L. Reed, Philos. Trans. R. Soc. London, Ser. A **355**, 1659 (1997).
[20] K. M. Dunn and K. Morokuma, J. Phys. Chem. **100**, 123 (1996).
[21] A. Golan, S. Rosenwaks, and I. Bar, J. Chem. Phys. **125**, 151103 (2006).
[22] S. J. Baek, K.-W. Choi, Y. S. Choi, and S. K. Kim, J. Chem. Phys. **117**, 10057 (2002).
[23] S. J. Baek, K.-W. Choi, Y. S. Choi, and S. K. Kim, J. Chem. Phys. **118**, 11040 (2003).
[24] S. J. Baek, K.-W. Choi, Y. S. Choi, and S. K. Kim, J. Chem. Phys. **118**, 11026 (2003).
[25] A. T. J. B. Eppink and D. H. Parker, Rev. Sci. Instrum. **68**, 3477 (1997).
[26] A. T. J. B. Eppink, B. Buijsse, M. H. M. Janssen, W. J. Zande, and D. H. Parker, J. Chem. Phys. **107**, 2357 (1997).
[27] V. Dribinski, A. Ossadtchi, V. A. Mandelshtam, and H. Reisler, Rev. Sci. Instrum. **73**, 2634 (2002).
[28] R. J. Bartlett, J. F. Stanton, J. Gauss, J. D. Watts, and P. G. Szalay, with contributions from A. A. Auer, D. B. Bernholdt, O. Christiansen, M. E. Harding, M. Heckert, O. Heun, C. Huber, D. Jonsson, J. Jusélius, W. J. Lauderdale, T. Metzroth, C. Michauk, D. P. O'Neill, D. R. Price, K. Ruud, F. Schiffmann, M. E. Varner, and J. Vásquez, ACES-II, (advanced concepts in electronic structure theory)-a product of the University of Florida, Quantum Theory Project (QTP). Integral packages included are VMOL (J. Almlof and P. R. Taylor), VPROPS (P. Taylor), and ABACUS (T. Helgaker, H. J. Ha Jensen, P. Jorgensen, J. Olsen, and P. R. Taylor).
[29] M. J. Frisch, G. W. Trucks, H. B. Schlegel *et al.*, GAUSSIAN 03, Revision B.03, Gaussian, Inc., Wallingford, CT, 2003.
[30] M. H. Park, K.-W. Choi, S. Choi, and S. K. Kim, J. Chem. Phys. **125**, 084311 (2006).
[31] D. H. Mordaunt, M. N. R. Ashfold, and R. N. Dixon, J. Chem. Phys. **104**, 6460 (1996).
[32] D. H. Mordaunt, R. N. Dixon, and M. N. R. Ashfold, J. Chem. Phys. **104**, 6472 (1996).
[33] A. Bach, J. M. Hutchison, R. J. Holiday, and F. F. Crim, J. Chem. Phys. **118**, 7144 (2003).
[34] A. Bach, J. M. Hutchison, R. J. Holiday, and F. F. Crim, J. Phys. Chem. A **107**, 10490 (2003).
[35] A. Bach, J. M. Hutchison, R. J. Holiday, and F. F. Crim, J. Chem. Phys. **116**, 9315 (2002).
[36] M. L. Hause, Y. H. Yoon, and F. F. Crim, J. Chem. Phys. **125**, 174309 (2006).
[37] Z. Lan, W. Domcke, V. Vallet, A. L. Sobolewski, and S. Mahapatra, J. Chem. Phys. **122**, 224315 (2005).